Control System Design of a H-shape configuration Fixed Wing VTOL based on a Patented Vertical Thrust System

Giorgio A. Orlando[1], Angelo Lerro[1] and Piero Gili[1]

[1]Mechanical and Aerospace Engineering Department, Polytechnic of Turin
giorgio.orlando@polito.it

Abstract

The study is dedicated to design a control architecture for a Lift+Cruise aircraft utilizing the patented ThrustPod technology. This innovative approach integrates Fixed Wing functionalities with retractable rotors to facilitate Vertical Take-Off and Landing. By transitioning between Multirotor and Fixed Wing modes, it enhances aerodynamic efficiency while preserving vertical flight capabilities. Using Incremental Nonlinear Dynamic Inversion, the control system autonomously manages each flight phase, supported by a state machine framework for mode transitioning. Through simulations based on realistic mission scenarios in mountain areas, the system demonstrates reliable performance across various flight regimes. The proposed integrated solution represents progress in Urban Air Mobility, potentially offering a practical transportation option for passengers and cargo in challenging environments.

1 Introduction

In recent years, advancements in energy storage, especially in battery capacities, alongside the evolution of Distributed Electric Propulsion (DEP), have ushered in a new era in transportation termed Urban Air Mobility (UAM). UAM, a key component of Advanced Air Mobility (AAM), expands beyond urban areas to encompass rural, regional, and subregional routes. DEP technology differs from conventional urban aircraft like helicopters by replacing a single large rotor with multiple smaller propellers, offering flexibility in design and layout. While the concept of UAM traces back to the 1980s in Europe with services like the Airlink shuttle, concerns regarding noise, pollution, safety, and stringent low-altitude flight regulations hindered its progress for years. However, recent interest and optimism have reinvigorated the field [2]. According to the European Union, urban populations have more than doubled over the past four decades and are projected to reach 5 billion by 2050 [4], raising concerns about future challenges such as traffic congestion and emissions. Innovative transportation solutions are imperative to address these impending urban challenges. The emergence of AAM introduces electric vertical take-off and landing (eVTOL) vehicles to utilize low-altitude airspace for transportation, potentially alleviating traffic congestion and pollution. These eVTOLs, designed to be low-noise, low-emission, safe, and cost-effective, offer promising alternatives [14]. Despite initial skepticism, the UAM industry is expected to experience significant growth by 2050, albeit with ongoing challenges in technology refinement and regulatory framework development [14]. Multicopters, leveraging DEP, represent an evolution in helicopter technology, ideal for urban environments due to their hovering and vertical flight capabilities. Unlike traditional helicopters, DEP technology allows for optimized designs without a large main rotorcraft. However, their flight efficiency is limited, affecting endurance, particularly for extended operations. To address this limitation, Fixed Wing eVTOLs combine vertical flight capabilities with fixed-wing cruising, enabling longer distances to be covered. However, flight dynamics become more complex, especially in the thrust vectoring subcategory, where optimizing each phase of flight is challenging. In the Lift+Cruise subcategory, where thrust and lift motors are separate, independently optimizing each phase becomes feasible. Yet, traditional Lift+Cruise vehicles may experience reduced aerodynamic efficiency due to additional aerodynamic drag caused by lift propellers. To overcome this challenge, an innovative solution based on patented ThrustPod (TP) technology will be introduced in the following section.

2 ThrustPod system

The ThrustPod innovative aerial platform features a unique design that merges the VTOL capabilities of Multirotor (MR) vehicles with the aerodynamic efficiency of fixed-wing flight. An essential aspect of this design is to maintain minimal interdependence between the two modes of operation, allowing for independent optimization of each state. To achieve this goal, the design eliminates the mechanical complexity associated with tilting surfaces [7]. The platform's hovering and vertical flight capabilities are provided by six ducted vertical lift propellers, which are exclusively used during VTOL phases. These lift propellers can be fully retracted within the fuselage during other operational phases to prevent aerodynamic performance degradation. The storage of lift motors within the main body is made possible by offsetting along the Z-axis the motors on one side of the longitudinal plane, enabling overlapping when retracted. The rotor extraction and retraction mechanism employs rails, ensuring extremely low energy consumption. The platform's wing-tail architecture is achieved through a boxed wing design aimed at reducing induced drag [7]. Aerodynamic control surfaces include elevators for pitch control and ailerons for roll control. Additionally, each wing features a horizontal thrust propeller, allowing for yaw control through differential thrust. This design choice eliminates the need for a vertical empennage. In summary, ThrustPod presents a pioneering approach to aerial platform design, combining VTOL and fixed-wing capabilities while prioritizing independent optimization and aerodynamic efficiency. The integration of lift propellers and the retraction mechanism contributes to the realization of a green and autonomous aircraft for Urban Air Mobility purposes.
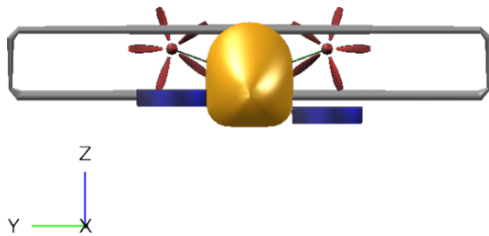

Figure 1: TP Front view

Figure 2: TP Isometric view

2.1 Mission overview

One of the key challenges in UAM is ensuring safe navigation within tight spaces, leading to two critical consequences: the necessity for Multirotor mode during vertical flight phases and strict size limitations. These constraints restrict the platform's capacity to a maximum of five passengers throughout various phases:

1. **Vertical Takeoff and Hovering**: The aircraft must vertically take off and hover until reaching the speed required for transitioning to fixed-wing mode.

2. **Climb**: Accelerating and ascending to an altitude of 3000 meters without pressurization.

3. **Cruise**: Covering the specified distance while maintaining a speed of 75 m/s.

4. **Descent**: Descending to the altitude for vertical landing.

5. **Hovering and Vertical Landing**: Transitioning back to MR mode, hovering, and achieving vertical landing.

Transitioning between MR and FW flight modes involves changing control variables. Therefore, an intermediary transition phase is essential to smoothly adjust the aircraft's state. Notably, lift motors are the most energy-intensive control component, emphasizing the importance of a quick transition.
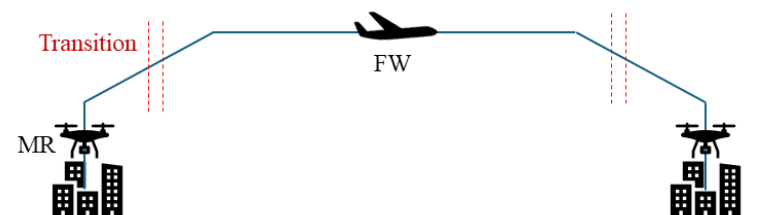

Figure 3: Mission Profile

2.1.1 State Machine and Controls

The mission profile can be segmented into three primary phases, with the platform conceptualized as a discrete state machine for control management. Each flight phase corresponds to a specific aircraft state, with transitions governed by predefined logic. To optimize energy usage, the system is discretized based on forward speed, aiming to transition to FW flight early to minimize battery weight. However, transitioning at low speeds poses challenges as aerodynamic lift alone may be insufficient for flight. To address this, a Transition or Hybrid mode (TR) is introduced between MR and FW modes, facilitating a seamless transition from vertical takeoff to cruising by adjusting control actions based on flight velocity [15]. The resulting state machine comprises:

1. Vertical flight phase $\rightarrow$ Multi-Rotor mode (MR) $\iff u < V_{tr_i}$.

2. Transition phase $\rightarrow$ Transition mode (TR) $\iff V_{tr_i} < u < K_S V_{st} = V_{tr_f}$.

3. Fixed Wing phase $\rightarrow$ Fixed-Wing mode (FW) $\iff u > V_{tr_f}$.

Where $K_S V_{st}$ represents the stall speed of the aircraft multiplied by a safety factor, and V_{tr_i}, V_{tr_f} denote the transition starting and ending velocities, respectively. In the Hybrid mode, control variables from both FW and MR modes coexist, addressing redundancy by distributing control actions based on current velocity. The transition function aims at ensuring smooth transitions between states by adjusting control load allocation. Boundary conditions at transition thresholds ensure a seamless shift between aircraft operational states.
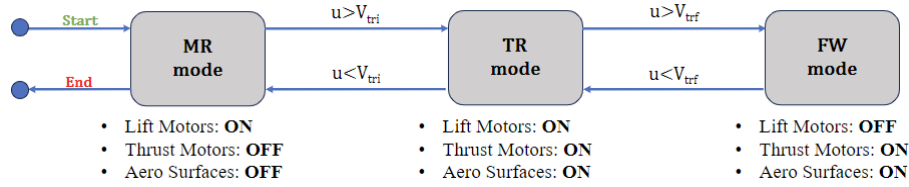

Figure 4: State machine

3   Mathematical Model

The vehicle's behavior is characterized by both kinematic and dynamic equations governing the rotational and transnational motion. The resulting nonlinear state space model is given as follows:

$$\begin{cases} \dot{\boldsymbol{V}}^B = -\boldsymbol{\omega}^B_{B/N} \times \boldsymbol{V}^B + \dfrac{1}{m}(\boldsymbol{F}^B_T + C_{B/N}(m\boldsymbol{g}^N) + C_{B/W}\boldsymbol{F}^W_A) \\ \dot{\boldsymbol{\Phi}} = T(\boldsymbol{\Phi})\boldsymbol{\omega}^B_{B/N} \\ \dot{\boldsymbol{\omega}}^B_{B/N} = (\mathbf{J}^B)^{-1}(-\boldsymbol{\omega}^B_{B/N} \times \mathbf{J}^B\boldsymbol{\omega}^B_{B/N} + \boldsymbol{M}^B_A + \boldsymbol{M}^B_T - \boldsymbol{G}^B) \\ \dot{\boldsymbol{P}}^N = C_{N/B}\boldsymbol{V}^B \end{cases} \tag{1}$$

The state is made of $\boldsymbol{V}^B$ denoting the velocity vector, $\boldsymbol{\omega}^B_{B/N}$ denoting the angular velocity vector of the body frame w.r.t. the inertial one, $\boldsymbol{\Phi}$ denoting the vector of Euler angles and $\boldsymbol{P}^N$ denoting the inertial position of the vehicle. $C_{B/N}, C_{B/W}, C_{N/B}$ represent Direction Cosine Matrices between different Cartesian Coordinate Systems. A linear aerodynamic model is employed for determining the aerodynamic actions ($\boldsymbol{F}^W_A$, $\boldsymbol{M}^B_A$), while Renard's formulas are leveraged for modeling thrust actions ($\boldsymbol{F}^B_T$, $\boldsymbol{M}^B_T$). Renard's coefficients are assumed to be constant and their value is determined from least squares fit of experimental data ([12],[9]). $\boldsymbol{G}^B$ denotes the gyroscopic effect ([10]), while m and $\boldsymbol{J}^B$ represent respectively the mass and the inertia matrix of the aircraft. The apex indicates the Cartesian Coordinate System in which each vector is described.

The actuators employed within the simulation process belong to two categories. Position servos (i.e. aerodynamic surfaces) are described by first order transfer functions in order to simulate the delay introduced by the actuators as in [19]. Velocity servos, indicating the motors, are modeled through a second order system made of an electrical circuit plus a mechanical rotating system as in [10].

4 Control Techniques

The control system design primarily relies on two nonlinear control techniques. Classical Nonlinear Dynamic Inversion (NDI) is utilized when equations are not influenced by model uncertainties, such as kinematics. In cases where uncertainties exist, Incremental Nonlinear Dynamic Inversion (INDI), its robust counterpart, is preferred.

4.1 Non-Linear Dynamic Inversion (NDI)

Nonlinear Dynamic Inversion has proven effective in controlling nonlinear systems while leveraging linear control techniques. Given a control-affine system in the form of:

$$\begin{cases} \dot{\boldsymbol{x}} = \boldsymbol{F}(\boldsymbol{x}) + \boldsymbol{G}(\boldsymbol{x})\boldsymbol{u} & \boldsymbol{x} \in \mathbb{R}^n, \boldsymbol{u} \in \mathbb{R}^m \\ \boldsymbol{y} = \boldsymbol{H}(\boldsymbol{x}) & \boldsymbol{y} \in \mathbb{R}^p \end{cases} \quad (2)$$

Each output y_i needs to be differentiated until the input $\boldsymbol{u}$ appears explicitly in the equation. Using the notion of Lie derivative ($L_f V(\boldsymbol{x}) = \frac{\partial V}{\partial \boldsymbol{x}} \boldsymbol{f}(\boldsymbol{x})$) and applying it to each output equation, we can obtain the following:

$$\begin{bmatrix} y_1^{r_1} \\ \vdots \\ y_p^{r_p} \end{bmatrix} = \begin{bmatrix} L_f^{r_1} H_1(\boldsymbol{x}) \\ \vdots \\ L_f^{r_p} H_p(\boldsymbol{x}) \end{bmatrix} + \begin{bmatrix} L_{g_1} L_f^{r_1-1} H_1(\boldsymbol{x}) & \cdots & L_{g_m} L_f^{r_1-1} H_1(\boldsymbol{x}) \\ \vdots & \ddots & \vdots \\ L_{g_1} L_f^{r_p-1} H_p(\boldsymbol{x}) & \cdots & L_{g_m} L_f^{r_p-1} H_p(\boldsymbol{x}) \end{bmatrix} \boldsymbol{u} = T_F(\boldsymbol{x}) + T_G(\boldsymbol{x})\boldsymbol{u} \quad (3)$$

Assuming T_G is invertible and defining $y_i^{r_i} = v_i$, $\forall i$ (v_i = i-th virtual input) the actual control variables u_i can be defined in terms of the virtual input v_i:

$$\boldsymbol{u} = T_G(\boldsymbol{x})^{-1}(\boldsymbol{v} - T_F(\boldsymbol{x})) \quad (4)$$

Since the virtual input v_i will act only on the output y_i the T_G matrix is knows as *decoupling matrix*. In this work, dynamic inversion will be used only for square systems where $r = r_1 + \cdots + r_p = n$. This case is simpler since there is no uncontrolled internal dynamics to be stabilized. Dynamic inversion is basically a change of coordinates that transforms a nonlinear system into a new linear one in which all the classical linear control methodologies can be applied. Defining $\boldsymbol{\mu}^T = [y_1, \cdots, y_1^{r_1-1}, \cdots, y_p, \cdots, y_p^{r_p-1}]$, the new linear system to be controlled is the following [16],[17]:

$$\begin{cases} \dot{\boldsymbol{\mu}} = A\boldsymbol{\mu} + B\boldsymbol{v} & \boldsymbol{\mu} \in \mathbb{R}^r, \boldsymbol{v} \in \mathbb{R}^p \\ \dot{\boldsymbol{y}}_{new} = \boldsymbol{\mu} \end{cases} \quad (5)$$

Nonlinear Dynamic Inversion offers effective control solutions for nonlinear dynamical systems. However, it has notable limitations as it requires the system to be affine in terms of control inputs and heavily relies on the accuracy of the mathematical model, making it sensitive to uncertainties arising from model mismatches [5].

4.2 Incremental Non-Linear Dynamic Inversion (INDI)

INDI addresses NDI's limitations through an incremental approach. This technique reduces dependence on precise mathematical models and enhances robustness to uncertainties and disturbances by leveraging sensor measurements, thus shifting the complexity of real-world dynamics away from equations and onto sensors. All unmodeled dynamics are introduced into the control law through actual state and state derivative measurements of the aircraft [18]. This method employs time-scale separation, grounded in the concept of control effectiveness, which measures how changes in control variables affect the system output. By extending this idea over time, it allows differentiation between slow and fast dynamics, based on the input's impact on the output within a small time interval [1]. In the most general case, we can assume to be dealing with a nonlinear, non control-affine dynamical system:

$$\dot{\boldsymbol{x}} = \boldsymbol{f}(\boldsymbol{x}, \boldsymbol{u}) \quad \boldsymbol{x} \in \mathbb{R}^n, \boldsymbol{u} \in \mathbb{R}^m \quad (6)$$

Under the assumption of infinitesimal time increment, we can expand the equation about the current point in time $(\boldsymbol{x}(t_0), \boldsymbol{u}(t_0))$:

$$\dot{\boldsymbol{x}} \approx \dot{\boldsymbol{x}}_0 + \nabla_{\boldsymbol{x}} \boldsymbol{f}_{(\boldsymbol{x}_0, \boldsymbol{u}_0)}(\boldsymbol{x} - \boldsymbol{x}_0) + \nabla_{\boldsymbol{u}} \boldsymbol{f}_{(\boldsymbol{x}_0, \boldsymbol{u}_0)}(\boldsymbol{u} - \boldsymbol{u}_0) \quad (7)$$

Given the assumption of quasi-instantaneous actuators, the control effectiveness of the input vector $\boldsymbol{u}$ is significantly greater than that of the state vector $\boldsymbol{x}$. Intuitively, this means that a change in the control input $\boldsymbol{u}$ has a much faster impact on the system compared to a change in the system state $\boldsymbol{x}$ itself, which translates in the following:

$$\nabla_{\boldsymbol{x}} \boldsymbol{f}_0 \Delta \boldsymbol{x} << \nabla_{\boldsymbol{u}} \boldsymbol{f}_0 \Delta \boldsymbol{u} \quad (8)$$

Considering full-state feedback and equating $\dot{x}$ to the virtual input v the control law becomes:

$$\boldsymbol{u} = \boldsymbol{u}_0 + (\nabla_{\boldsymbol{u}} \boldsymbol{f}_0)^{\dagger}(\boldsymbol{v} - \dot{\boldsymbol{x}}_0) \tag{9}$$

The expression reveals several significant insights:

- Linearization around the current time point enables the technique's application to non-affine systems.

- The Moore-Penrose (MP) inverse of the Control Effectiveness Matrix broadens applicability to non-square or non-invertible systems, with potential optimization solutions for control constraints, especially in systems with redundant actuators [8],[13],[11].

- Plant knowledge is confined to the Control Effectiveness Matrix, even adaptable online for enhanced robustness [18],[3]. The system's remainder is inferred from acceleration and actuator output measurements, with model inaccuracies compensated through sensor feedback.

- Variables with subscript '0' must be measured or estimated. Angular accelerations, typically inaccessible via conventional IMUs, necessitate estimation from rate measurements.

- Delay poses a primary challenge in Incremental Nonlinear Dynamic Inversion, attributed mainly to actuator dynamics, filtering for pseudo-differentiation, and inherent sensor delays [20].

5 Control System Design

This section represents a transition from theoretical control principles to their practical application, providing insights into the design of control systems utilizing INDI. It outlines the development of dedicated controllers for MR, FW, and TR modes, offering a glimpse into the process without delving into mathematical details.

5.1 Inner Loop Design

The inner loop remains consistent across all three states of the aerial platform. Variations in gains will solely apply to the MR mode. The primary objective of the inner loop is to achieve a desired attitude expressed in terms of Euler angles, denoted as $\boldsymbol{\Phi} = [\phi, \theta, \psi]^T$. It is of paramount importance that the inner loop operates at a higher frequency than the outer loop. Indeed, in cascaded control with time scale separation, the entire inner loop should effectively act as an actuator for the outer loop.
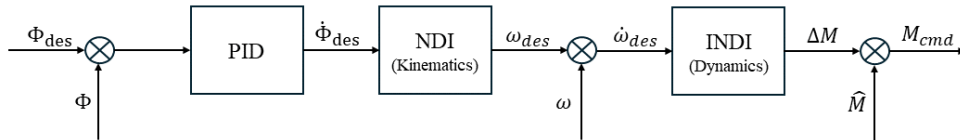

Figure 5: Inner Loop Control System

5.1.1 NDI for attitude kynematics

As stated earlier, for rotational kinematics classical NDI is sufficient since no model uncertainties are present [8]. Rearranging (1) it is possible to derive the following control law:

$$\boldsymbol{\omega}_{B/N_{des}}^B = T(\boldsymbol{\Phi})^{-1} \boldsymbol{\Phi}_{des} \tag{10}$$

With the virtual input $\boldsymbol{\Phi}_{des}$ being provided through a linear controller.

5.1.2 INDI for rotational dynamics

Assuming gyroscopic effects are negligible, the rotational dynamics from (1) can be manipulated with the INDI approach to yield:

$$\Delta \boldsymbol{u} = \mathbf{J}^B(\boldsymbol{v} - \dot{\boldsymbol{\omega}}_{B/N_0}^B) \tag{11}$$

Where the virtual input $\boldsymbol{v}$, like for NDI, can be designed using any linear control techniques.

5.2 Outer Loop Design

The outer loop control system plays a key role in tracking a specified trajectory based on inertial position. It receives velocity directives from a guidance algorithm and then issues desired attitude instructions to the inner loop, along with desired forces to an allocation algorithm. Unlike MR mode, where sustained flight relies on the orientation of the vertical thrust vector for translational motion, FW and TR modes share a similar control structure tailored for their respective flight characteristics.

5.2.1 MR mode

The outer loop adopts a similar approach to designing the controller as the inner loop, focusing on the translational dynamics within the INDI framework. Given the time scale difference between the loops, the attitude is treated as a control input operating alongside the motors' time scale. Thus, the controller output includes both the desired attitude for the inner loop and the desired thrust along the Z_B axis for feeding into an allocation algorithm.

5.2.2 FW/TR mode

The outer loop during FW/TR mode adopts a distinct approach compared to the MR phase, aiming to maintain a zero Angle of Sideslip (β) to optimize flight efficiency and mitigate the Dutch Roll phenomenon. To accomplish this objective, a sideslip controller is implemented, as described in [6]. Moreover, in fixed-wing flight, turning primarily relies on the roll angle (ϕ). Consequently, the azimuth angle χ_{ref} derived from the outer loop is converted into a reference roll angle (ϕ_{ref}) using a linear controller. Similarly, a PID controller is utilized to determine the reference pitch based on the flightpath angle. The differentiation between TR and FW modes lies in the application of INDI. In FW mode, translation is regulated solely through T_x, allowing robust inversion to be applied to the single dynamical equation along X_B. Conversely, TR mode utilizes both T_x and T_z, necessitating simultaneous inversion of the entire longitudinal dynamics.

6 Simulations

The simulation endeavors to present the outcomes of a comprehensive mission that encompasses transitions across different states. Although not explicitly detailed in the work, each controller has undergone rigorous individual validation. The critical focus now lies in assessing the controllers' capability to smoothly transition between control variables and states during real-world operations. In the context described, "forward transition" refers to the acceleration phase and comprises two distinct state changes: MR $\rightarrow$ TR and TR $\rightarrow$ FW.

6.1 MR $\rightarrow$ TR

During the MR to TR transition, aerodynamic surfaces and thrust motors are activated. This causes the vehicle to tilt backward as forward propulsion shifts to thrust motors while vertical traction counteracts gravity.
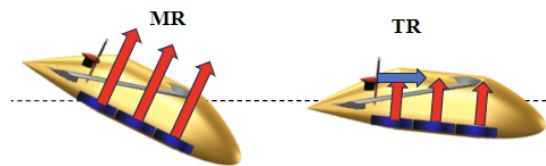

Figure 6: MR to TR

A state machine approach dictates an on-off behavior for FW control variables, resulting in a rapid change in pitch reference. To mitigate this, a limiter on the reference pitch rate is implemented. The transition leads to a slight increase in altitude due to the upward pitching motion, aligning the vertical thrust with the local vertical and causing a temporary surge in upward force.

6.2 TR $\rightarrow$ FW

The following transition involves gradually deactivating the lift motors using an exponential decay function, chosen for its smoother and more controlled effect compared to a binary on-off mechanism. As the upward force decreases,
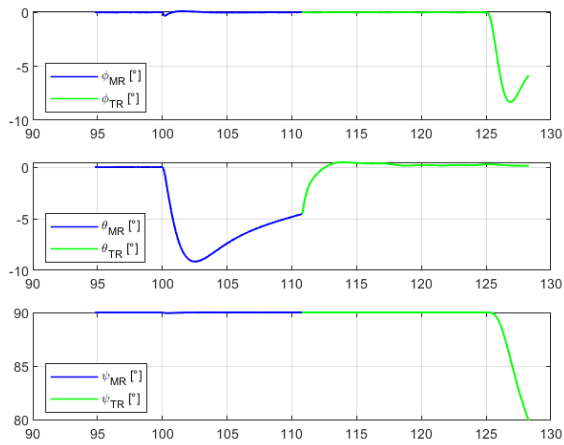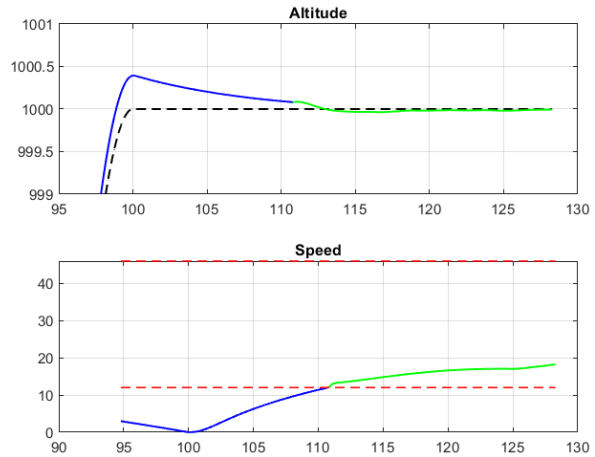
Figure 7: Φ for switch n.1

Figure 8: h and V vs t for switch n.1

there may be a corresponding decrease in altitude. To offset this, the vehicle is anticipated to adjust its Angle of Attack (AoA) to generate additional aerodynamic lift.
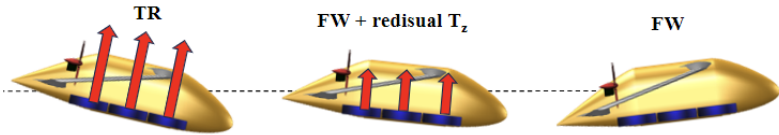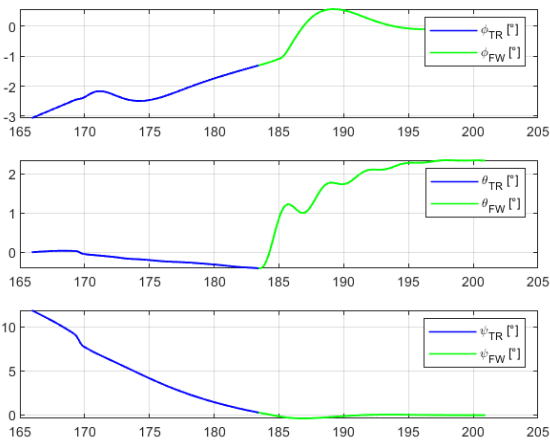

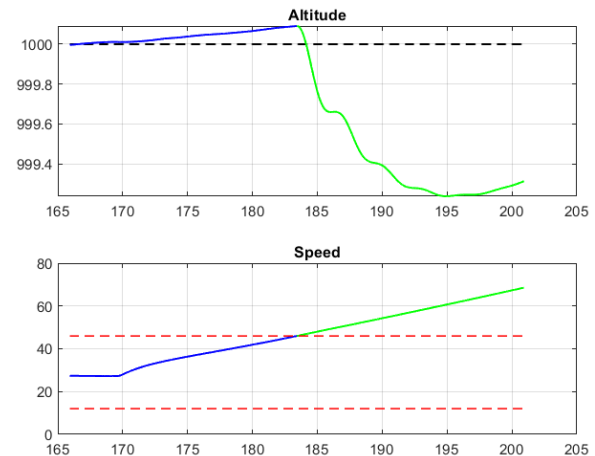Figure 9: TR to FW

Figure 10: Φ for switch n.1

Figure 11: h and V vs t for switch n.1

Similar logic can be extended to the backward transition process.

6.3   Simulation of mission in mountainous terrains

In this section, we delve into the practical application of TP technology, highlighting its potential to address challenges encountered by mountain communities. Collaborating with UNCEM (the National Union of Mountain Communities), Politecnico envisions leveraging this technology to overcome issues in remote areas by proposing the deployment of STOL (Short Takeoff and Landing) vehicles. Unlike traditional cable car systems, which can be costly and susceptible to weather disruptions, STOL vehicles offer a promising alternative. They require minimal infrastructure and can utilize available spaces as makeshift runways, potentially reducing costs and

enhancing adaptability. Furthermore, the ample space in mountainous regions allows for the repurposing of suitable airstrips or landing zones for STOL vehicles, offering greater flexibility during adverse weather conditions and improving transportation reliability. This approach represents a cost-effective and weather-resilient solution, leveraging existing open spaces to enhance accessibility and transportation options for both goods and people in remote mountainous regions. The simulation focuses on a selected route connecting two Italian mountain towns, Balme and Ceres, with different altitudes, encompassing various mission phases despite the relatively short ground distance between them. The route was planned by marking specific waypoints along the river's path. Wind disturbances in the simulation were generated based on the prevailing wind conditions in the two cities ([21],[22]), helping to simulate realistic wind scenarios for the given areas.
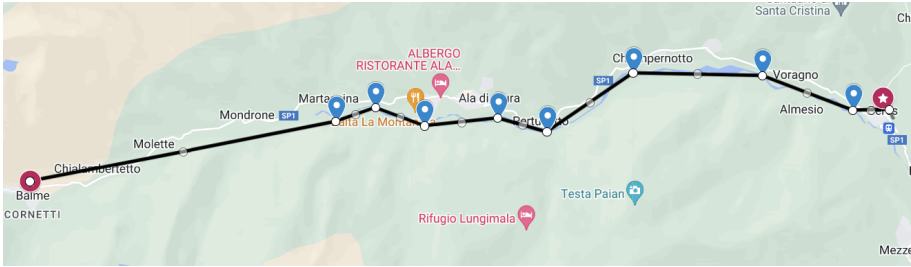

Figure 12: Ceres-Balme route

Below the 3D and ground track trajectories of the aircraft are compared with the reference ones.
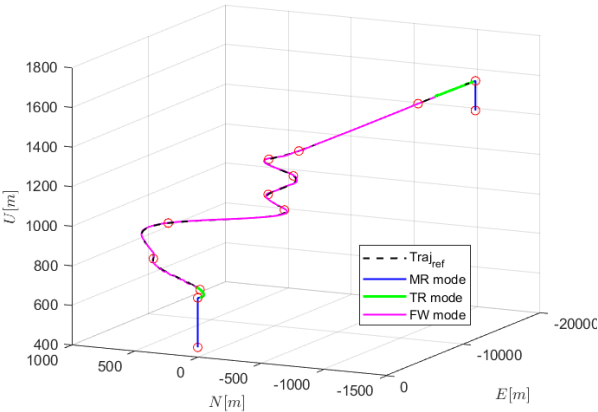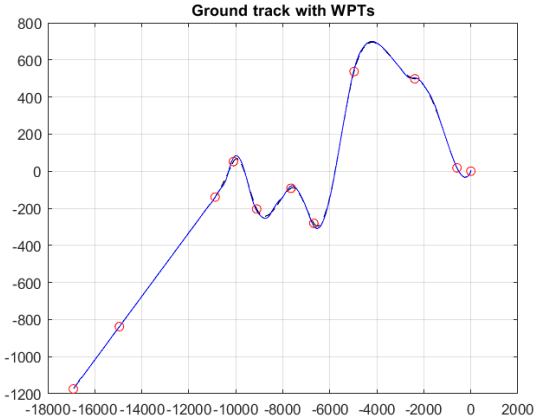

Figure 13: 3D Trajectory

Figure 14: Ground Track

However, to actually see the effect of wind disturbances on such a long period of time, it is necessary to plot also the inertial position error for each axis of the linear motion.
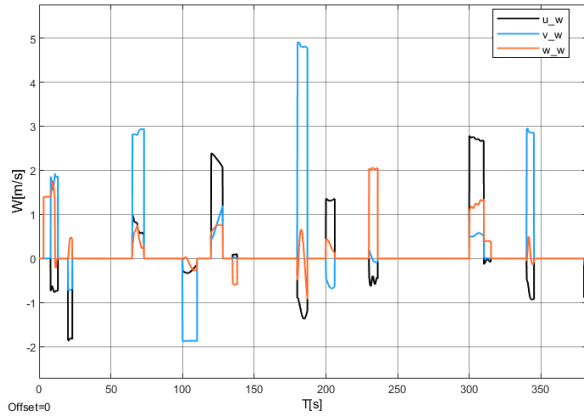
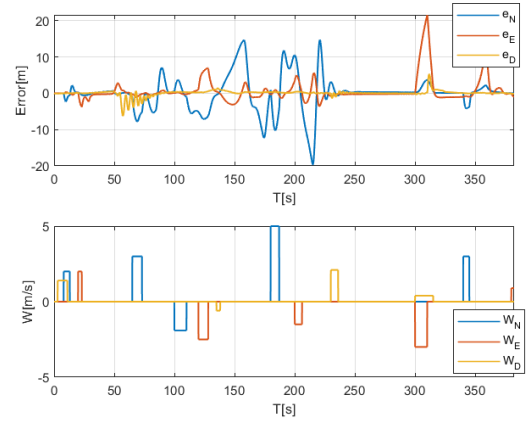Figure 15: Wind Disturbances in Body Components

Figure 16: Position Error vs Inertial Wind Disturbances

In summary, the aircraft effectively completes the mission, overcoming sudden wind disturbances and maneuvering through challenging turns along the riverbed. It's crucial to emphasize that the main goal was to validate the vehicle's capability to navigate demanding routes, rather than to optimize the trajectory. Therefore, the aircraft's performance indicates its readiness to handle smoother and more efficient trajectories in upcoming missions.
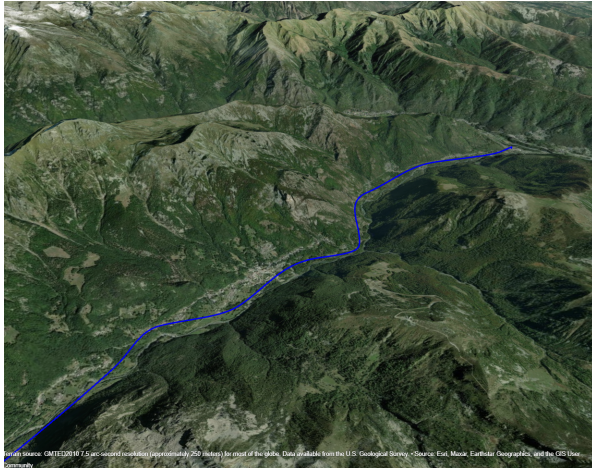

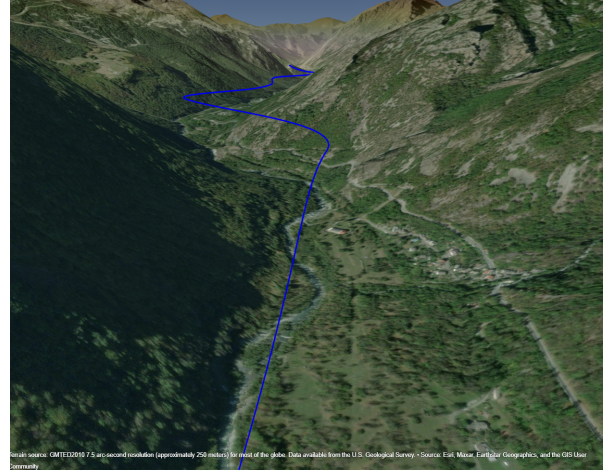Figure 17: View 1 of simulated trajectory imprinted on satellite images

Figure 18: View 2 of simulated trajectory imprinted on satellite images

7 Conclusions

The current study provides a promising framework for future advancements in Urban Air Mobility by demonstrating the effectiveness of Incremental Nonlinear Dynamic Inversion and state machine frameworks in managing flight mode transitions. Moving forward, optimizing control allocation algorithms could further enhance the transition process, ensuring smoother and more efficient operations. By integrating optimal control allocation techniques, the system could dynamically distribute control inputs to maximize performance during critical phases like transitioning between Multirotor and Fixed Wing modes. This approach holds potential for improving the reliability and agility of UAM vehicles, contributing to the evolution of urban aerial transportation.

References

[1] Year of access: 2023. URL: http://www.aerostudents.com/courses/advanced-flight-control/nonlinearDynamicInversion.pdf.

[2] Raul Batlle. "The potential of deploying Urban Air Mobility services as an integrated transport system: a London area case study". PhD thesis. Aug. 2020. DOI: 10.13140/RG.2.2.29467.80163.

[3] J. Chang et al. "Predictor-based Adaptive Incremental Nonlinear Dynamic Inversion for Fault-Tolerant Flight Control". In: *IFAC PapersOnLine* 55-6 (2022), pp. 730–736.

[4] *Continuing Urbanisation*. European Commission's Knowledge for Policy. Year of Access: 2023. URL: https://knowledge4policy.ec.europa.eu/continuing-urbanisation_en.

[5] R. da Costa, Q. Chu, and J. Mulder. "Reentry Flight Controller Design Using Nonlinear Dynamic Inversion". In: *Journal of Spacecraft and Rockets* 40.1 (2003), pp. 64–71. DOI: 10.2514/2.3916.

[6] Zhou L. et al. "Incremental nonlinear dynamic inversion based path-following control for a hybrid quad-plane unmanned aerial vehicle". In: *Int J Robust Nonlinear Control* (2022), pp. 1–24. DOI: 10.1002/rnc.6503.

[7] A. Lerro, L. Nanu, and P. Gili. "ThrustPod: a novel solution for vertical take-off and landing systems". In: *Proceedings of the DICUAM 2022 Conference* (Mar. 2022).

[8] Z. Liu et al. "VTOL UAV Transition Maneuver Using Incremental Nonlinear Dynamic Inversion". In: *International Journal of Aerospace Engineering* 2018 (). DOI: 10.1155/2018/6315856.

[9] Maccotta M. *Multirotor UAVs for fugitive emissions detection: sizing, modeling and control system desgin*. 2018.

[10] M. Moussid, A. Sayouti, and H. Medromi. "Dynamic Modeling and Control of HexaRotor using Linear and Nonlinear Methods". In: *International Journal of Applied Infomation Systems(IJAIS)* 9.5 (Aug. 2015). ISSN: 2249-0868.

[11] O. Pfeifle and W. Fichter. "Minimum Power Control Allocation for Incremental Control of Over-Actuated Transition Aircraft". In: *Journal of Guidance, Control, and Dynamics* (Nov. 2022).

[12] S. K. Phang, S. Z. Ahmed, and M. R. A. Hamid. "Design, Dynamics Modelling and Control of a H-Shape Multi-rotor System for Indoor Navigation". In: *Proceedings of the 1st International Conference on Unmanned Vehicle Systems(UVS)* (Feb. 2019).

[13] T. M. L. De Ponti. *Incremental Nonlinear Dynamic Inversion Controller for a Variable Skew Quad Plane*. 2022.

[14] PWC Strategy&. *The path towards a mobility in the third dimension: How to create a National ecosystem for Advanced Air Mobility*. Insight Report. PWC Strategy&, 2021. URL: https://www.strategyand.pwc.com/it/en/assets/pdf/S&-path-towards-a-mobility-in-the-third-dimension.pdf.

[15] Mao S et al. "Linear-Active-Disturbance-Rejection-Based Vertical Takeoff and Acceleration Strategy with Simplified Vehicle Operations for Electric Vertical Takeoff and Landing Vehicles". In: *Mathematics* (2022). DOI: 10.3390/math10183333.

[16] F. Sabatino. *Quadrotor Control: modeling ninlinear control design and simulation*. 2015.

[17] Slotine and Li. *Applied Nonlinear Control*. Pearson College Div., 1990.

[18] Smeur, Chu, and de Croon. "Adaptive Incremental Nonlinear Dynamic Inversion for Attitude Control of Micro Air Vehicles". In: *Journal of Guidance, Control, and Dynamics* 39.3 (Mar. 2016). DOI: 10.2514/1.G001490.

[19] Brian L. Stevens, Frank L. Lewis, and Eric N. Johnson. *Aircraft Control and Simulation*. Wiley, 2006.

[20] R. C. van't Veld. *Incremental Nonlinear Dynamic Inversion Flight Control: Stability and Robustness Analysis and Improvements*. 2016.

[21] *www.meteoblu.com*. Accessed in 2023. URL: https://www.meteoblue.com/it/tempo/historyclimate/climatemodelled/ceres_italia_3179099.

[22] *www.meteoblu.com*. Accessed in 2023. URL: https://www.meteoblue.com/it/tempo/historyclimate/climatemodelled/balme_italia_3182446.